NANO LETTERS

pubs.acs.org/NanoLett

Letter

Perspiration-Wicking and Luminescent On-Skin Electronics Based on Ultrastretchable Janus E-Textiles

Jiancheng Dong, Yidong Peng, Lei Pu, Kangqi Chang, Le Li, Chao Zhang, Piming Ma, Yunpeng Huang,* and Tianxi Liu*

Cite This: *Nano Lett.* 2022, 22, 7597−7605

Read Online

ACCESS | Metrics & More | Article Recommendations | Supporting Information

ABSTRACT: Stretchable electronics have attracted surging attention for next-generation smart wearables, yet traditional flexible devices fabricated on hermetical elastic substrates cannot satisfy lengthy wearing comfort and signal stability due to their poor moisture and air permeability. Herein, perspiration-wicking and luminescent on-skin electrodes are fabricated on superelastic nonwoven textiles with a Janus configuration. Through the electrospin-assisted face-to-face assembly of all-SEBS microfibers with differentiated diameters and composition, porosity and wettability asymmetry are constructed across the textile, endowing it with antigravity water transport capability for continuous sweat release. Also, the phosphor particles evenly encapsulated in the elastic fibers empower the Janus textile with stable light-emitting capability under extreme stretching in a dark environment. Additionally, the precise printing of highly conductive liquid metal (LM) circuits onto the matrix not only equips the electronic textile with broad detectability for various biophysical and electrophysiological signals but also enables successful implementation of human−machine interface (HMIs) to control a mechanical claw.

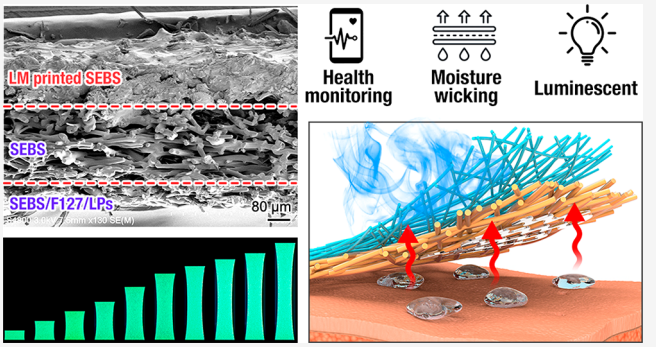

KEYWORDS: *bioelectrode, Janus textile, perspiration-wicking, personal health monitoring, liquid metal*

The rapid development of artificial intelligence and the Internet of things (IoT) is updating our lifestyle in a noticeable way, and the cornerstone of these technologies is the powerful and accurate communication between humankind and machines.[1−5] Particularly, deformable on-skin electronics are becoming the primary interactive medium for next-generation HMIs to meet the needs of stretchability, portability, and low power consumption.[6−8] Deformable electronics generally consist of stretchable substrates assembled with flexible circuits. Yet conventional wearable devices are usually made up of rigid, brittle, and hermetical matrixes that cannot realize the intimate contact with human skin nor satisfy long-term wearing comfort. Fortunately, elastic microfibers/textiles with porous networks, high specific area, and a low Young's modulus perfectly meet the requirements to develop comfortable and conformable wearing electronics.[9−13] Additionally, visualized stretchable electronics with human-readable visual optical signals have attracted considerable research interest due to the highly efficient human−machine dialogue in solid-state lighting, displays, and biomedicine.[14−16] So far, the reported visualized electronic skins are mainly focused on electroluminescence[17,18] and mechanoluminescence.[19] Nevertheless, the development of the mechano-/electro-induced luminescent devices ineluctably implicates complicated preparation processes, high cost, and an external power supply (e.g., electroluminescent devices require voltage higher than 1 kV).[20] On the other side, long persistent luminescence (LPL) materials were considered as promising alternatives in the development of visualized electronics owing to their superior luminescence properties including efficient excitations[21] and hours-long highly visible afterglow.[22] Upon exposure to ultraviolet or visible light, LPL materials absorb the excitation energy and release the energy very slowly (over 10 h) as colored light.[23] Moreover, because human naked eyes possess the maximum vision sensitivity at about 555 nm in photopic vision, LPL materials with emission peaks in the green spectral region are always desirable for safety signage and night-vision displays.[24,25]

In this research, an ultrastretchable and perspiration-wicking electronic textile with long persistent luminescence was developed for comprehensive personal health monitoring and HMIs. Combining an efficient electrospin-assisted face-to-face assembly and stencil printing of highly conductive liquid metal

Received: July 6, 2022
Revised: August 28, 2022
Published: September 9, 2022

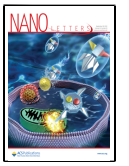

https://doi.org/10.1021/acs.nanolett.2c02647
Nano Lett. 2022, 22, 7597−7605

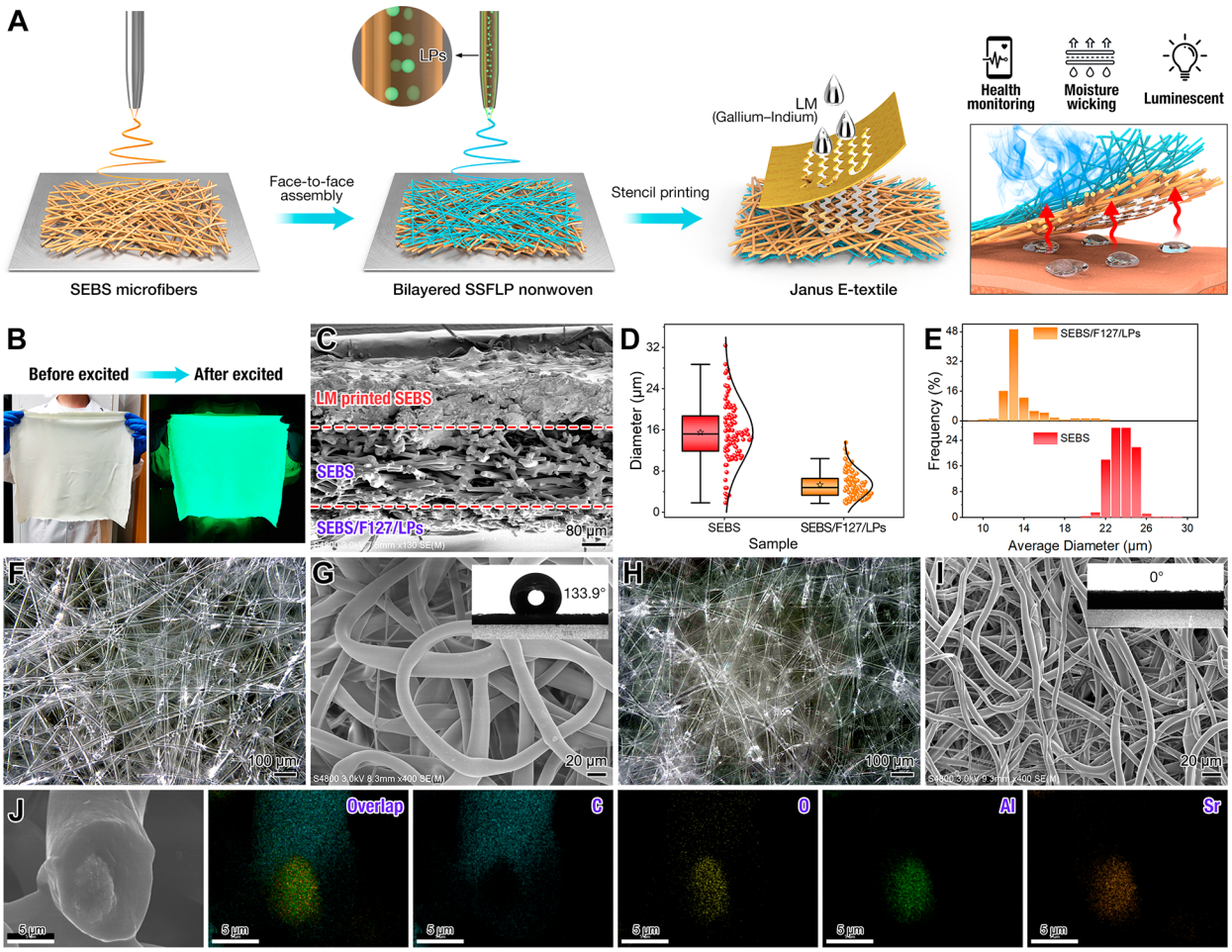

Figure 1. (A) Fabrication process of the ultrastretchable Janus E-textile. (B) Digital photographs of the fabricated large-size Janus E-textile with luminescent capability. (C) The cross-sectional SEM image of the Janus E-textile. (D,E) Diameter and pore size distribution of pure SEBS and SEBS/F127/LPs (LPs content: 30 wt %) microfibers. Optical microscope and SEM images of (F,G) pristine SEBS and (H,I) SEBS/F127/LPs (LPs content: 30 wt %) microfibers (insets showing the corresponding WCAs). (J) Elemental mapping of a single SEBS/F127/LPs fiber.

circuits, a Janus nonwoven textile with asymmetric porosity and wettability along the thickness was obtained based on tailored fiber sizes and compositions, allowing the bilayered nonwoven textile with unidirectional sweat transporting capability under large-scale deformation. Meanwhile, the luminescent $SrAl_2O_4$: Eu^{2+}, Dy^{3+} particles embedded in the SEBS microfibers even equipped the Janus textile with night-vision displays. Finally, a gallium−indium eutectic LM circuit was stencil-printed to endow the elastic textile with stable electrical conductivity under extreme elongation. As a result, the as-developed Janus E-textiles can be directly applied as comfort-wearing epidermal bioelectrodes to monitor biomechanical and bioelectric signals of the human body, which also can be further utilized to manipulate a mechanical claw. Therefore, this work provides a feasible solution for the development of visualized stretchable electronics, which can be extended to other multifunctional sensing devices.

Design of the Janus E-Textile. The fast advancement of wearable electronics imposes challenges on the epidermal devices for their wearing comfort and functionality under complex deformation including torsion, bending, and folding. Specifically, several key factors should be taken into account to satisfy the comfort necessity of on-skin electrodes during long-term mounting. First, adequate hardness (comparable to human skin) and skin conformability ought to be fulfilled to realize the intimate contact between epidermal devices and the skin.[26−28] Next, satisfactory stretchability (above ∼80%) is indispensable to sustain large skin and joint deformation and to avoid measurement artifacts caused by relative slippage of the devices.[29] It is equally important that on-skin devices should be permeable so as to maintain the air and moisture exchange between the skin and ambient environment, yet it is still hard for present wearable electronics to fulfill these characteristics synchronously.[30] Here, hydrogenated SEBS with a skin-like modulus was selected and fabricated into porous fibrous nonwoven textiles via electrospinning, thus providing a breathable, soft, and stretchable matrix that perfectly satisfies the requirements of wearable on-skin electronics. Moreover, perspiration accumulation in conventional porous epidermal devices always causes uncomfortable sticky feelings and health issues during strenuous exercises and outdoor activities. It has been proved that permeable membranes with asymmetric wettability show great ability for unidirectional water transport and can pump sweat from one side to the other automatically.[31] This work took advantage of such a structure via the tight assembly of a superhydrophilic SEBS/F127 layer and hydrophobic SEBS layer to construct functional textiles with reserve wettability. On the other side, a low-cost yet highly efficient commercial LPL material, $SrAl_2O_4$: Eu^{2+}, Dy^{3+} ,was incorporated into the

https://doi.org/10.1021/acs.nanolett.2c02647
Nano Lett. 2022, 22, 7597−7605

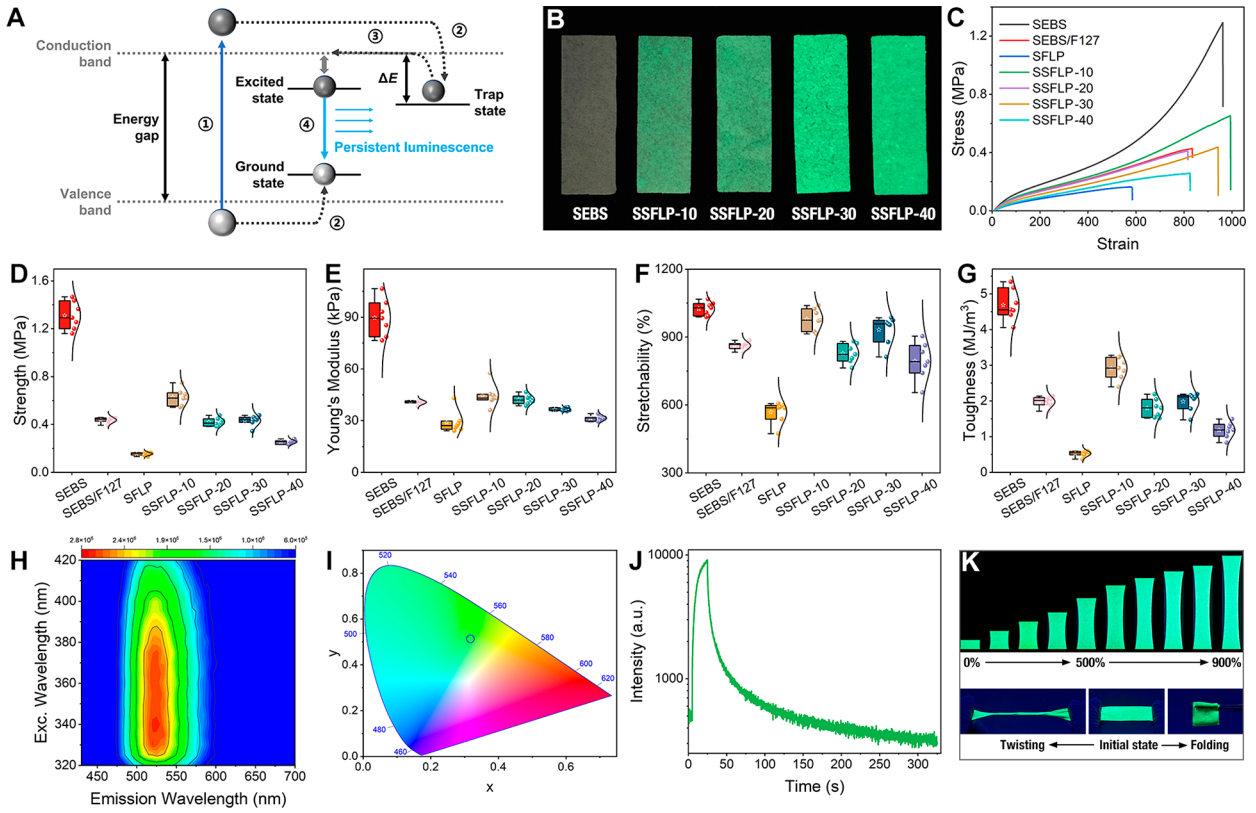

Figure 2. (A) Luminescence mechanism of $SrAl_2O_4$: Eu^{2+}, Dy^{3+}. (B) Digital photographs of SEBS and excited Janus SSFLP textiles. (C) Strain−stress curves, (D) strength, (E) Young's modulus, (F) stretchability, and (G) toughness diagrams of the pristine SEBS, SEBS/F127, SEBS/F127/LPs (SFLP), and different SSFLP textiles. (H) Excitation−emission map, (I) CIE 1931 color space diagram, and (J) photoluminescence lifetime of the SSFLP-30 Janus textile. (K) Digital photographs of luminescent SSFLP-30 under 900% elongation and various levels of mechanical torture.

fibrous matrix to endow the textile with a long-persistent phosphorescence function. Figure 1A schematically illustrates the preparation of the highly stretchable, perspiration-wicking, and luminescent Janus SSFLP textile.

Thanks to the facile electrospin-assisted face-to-face assembly method as well as the low-cost raw materials, the large-scale luminescent SSFLP electronic textiles are ready to be produced as shown in Figure 1B. The typical cross section morphology of SSFLP is shown in Figure 1C; it can be observed that the LM is homogeneously distributed on the SEBS layer. Moreover, the diameter and pore size distributions of each layer were measured and summarized in Figure 1D,E; the diameter of SEBS microfibers significantly decreased from 15.48 ± 5.92 to 5.32 ± 2.59 μm after blending with F127 and LPs (30 wt %), accordingly. The mean pore size also decreased from 24.05 to 13.57 μm, exhibiting the well-defined asymmetric configuration. Furthermore, the first layer of SEBS microfibers possesses highly porous microstructures with transparent and smooth fibers under microscope observations as shown in Figure 1F,G. Plus, the SEBS layer showed an intrinsic hydrophobic property with a water contact angle (WCA) up to 133.9° (inset of Figure 1G). SEBS/F127/LPs microfibers still maintained a transparent appearance for better luminescence emission, which also exhibited a complete superhydrophilicity surface with a WCA of nearly 0° attributed to the abundant hydroxyl groups on F127 (Figure 1H,I). Moreover, the elemental mapping further verifies the uniform distribution of Al, O, and Sr elements on the cross section of SEBS/F127/LPs microfibers (Figure 1J), indicating the phosphors are well-encapsulated in the SEBS/F127 matrix, ensuring their stability for long-term applications.

Luminescent Properties of the Janus E-Textile. Persistent luminescence has many well-known applications in diverse scenarios including bioimaging, biosensing, safety signage, and night-vision displays.[21] The luminescence of $SrAl_2O_4$: Eu^{2+}, Dy^{3+} can be explained by the electron model in Figure 2A. Figure 2B shows the digital photo of the neat SEBS nonwoven and the excited Janus textiles (λ_{ex}= 365 nm), revealing the uniform luminescence emission owing to the strong and durable luminescence of $SrAl_2O_4$: Eu^{2+}, Dy^{3+} and the transparent characteristics of the SEBS/F127 matrix. Apparently, more LPs addition gave rise to brighter luminescence; however, it would inevitably cause mechanical performance degradation. Reliable mechanical strength is essential for the long-term operation stability of epidermal electronics. A series of tensile tests were conducted to evaluate the comprehensive mechanical performances of the fabricated nonwoven textiles (detailed discussion on Figure 2C−G is in the Supplementary Discussion). Thus, through an electrospin-assisted face-to-face assembly of the robust SEBS microfibers and the low-modulus SEBS/F127/LPs fibers, a Janus nonwoven textile with neutralized yet well-rounded mechanical performance can be readily obtained. As revealed in Figure 2C−G, the Janus SSFLP textiles with addition of different LPs show a skin-like modulus, high stretchability of around 900%, and appropriate toughness, which perfectly satisfy the requirements raised by wearable epidermal electronics. Notably, the strength, Young's modulus, and toughness of SSFLP gradually decrease with the loading content of LPs.

https://doi.org/10.1021/acs.nanolett.2c02647
Nano Lett. 2022, 22, 7597−7605

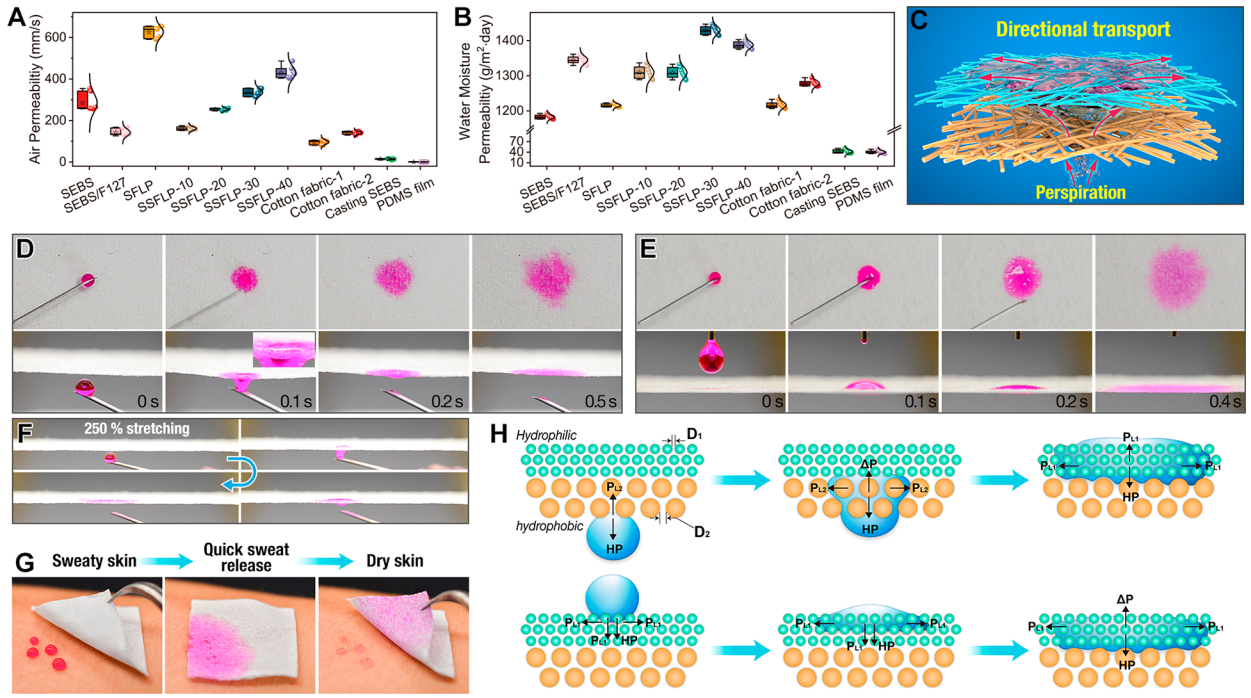

Figure 3. (A) Air and (B) water moisture permeability of pristine SEBS, SEBS/F127, SEBS/F127/LPs, and SSFLP nonwoven textiles. (C) Schematic depicting the directional perspiration transport across the Janus textile. Wetting behavior (rhodamine B, 50 μL) of the (D) SEBS side and (E) SEBS/F127/LPs side observed from the top and the side views. (F) Antigravity liquid self-pumping in the Janus textile under 250% stretching. (G) Practical application of the Janus textile on perspiration-wicking. (H) Diagrams illustrating the simplified perspiration-wicking process in the Janus E-textile.

Considering the luminescent property as well as the comprehensive mechanical performance, SSFLP-30 bilayered textiles were selected as the optimized sample for the following experiments.

The luminescent properties of Janus SSFLP-30 textiles were further studied. First, excitation-phosphorescence emission mapping measurements were carried out to understand the luminescent property (Figure 2H). Clearly, the bilayered nonwoven shows an excitation wavelength ranging from 325 to 415 nm, while the excitation wavelength range is 490−565 nm. The full width at half maxima (fwhm) of the Janus textile was measured to be 79 nm, generating the yellow-greenish color. The emission color was also confirmed by Commission Internationale de L'Eclairage (CIE) diagram (Figure 2I), indicating the color coordination of obtained luminescent microfibers was (x: 0.317, y: 0.513). Figure 2J presents the photoluminescence lifetime decay of the Janus textile (λ_{ex} = 365 nm, λ_{em} = 535 nm) at ambient temperature. It was found that the after-glow decay curve can be well-fitted by the triexponential formula (R^2 = 0.996):[32]

$$I(t) = I_0 + A_1\exp\left(-\frac{t}{\tau_1}\right) + A_2\exp\left(-\frac{t}{\tau_2}\right) + A_3\exp\left(-\frac{t}{\tau_3}\right) \quad (1)$$

which unveiled the fast-decay component (time-τ_1), the intermediate-decay component (time-τ_2), and the slow-decay component (time-τ_3). Thus, the mean photoluminescence lifetimes (τ_{ave}) of the Janus textile can be calculated by the following equation:

$$\tau_{ave} = \sum A_i\tau_i^2 / \sum A_i\tau_i \quad (2)$$

According to the fitted curve, τ_1, τ_2, and τ_3 were determined to be 0.67, 6.73, and 55.56 s, respectively; hence, the photoluminescence lifetime was calculated to be 41.36 s for the LPs-embedded bilayered microfibers. Whereas the raw phosphor particles show a lifetime of 58.28 s (Figure S2), significant lifetime decay can be ascribed to the influence of organic solvent. The light-emitting property of the Janus textile was also confirmed under harsh mechanical deformations. As can be seen in Figure 2K and Video S1, contributing to the excellent luminescence of $SrAl_2O_4$: Eu^{2+}, Dy^{3+} and the stable encapsulation of a robust SEBS matrix, the Janus textile exhibited a uniform and bright emission during the continuous stretching up to 900% and under extreme twisting and complete folding. Thus, the fabricated on-skin luminescent electronics can accommodate complex application scenarios.

Perspiration-Wicking Properties of the Janus E-Textile. The Janus textile manifests extraordinary moisture and air permeability to regulate the human skin microenvironment (Figure 3A,B, a detailed discussion is provided in the Supplementary Discussion). More importantly, the bilayered structure of Janus SSFLP textile creates a capillary pressure difference owing to the asymmetric fiber diameters and pore sizes; the superhydrophilic SEBS/F127/LPs layer can further absorb and diffuse the perspiration from the hydrophobic SEBS layer, boosting sweat vaporization from human skin (Figure 3C). The typical perspiration-wicking performance can be evaluated by observing the water (50 μL, dyed with rhodamine B) transport process through the bilayered textiles from the side and top view, respectively (Figure 3D,E, Videos S2 and S3). When dyed water was dropped on the SEBS layer, the droplet can penetrate the textile immediately and transport to the upper SEBS/F127/LPs layer in less than 0.1 s. Whereas, the water cannot pass through the textile when it was dropped

https://doi.org/10.1021/acs.nanolett.2c02647
Nano Lett. 2022, 22, 7597−7605

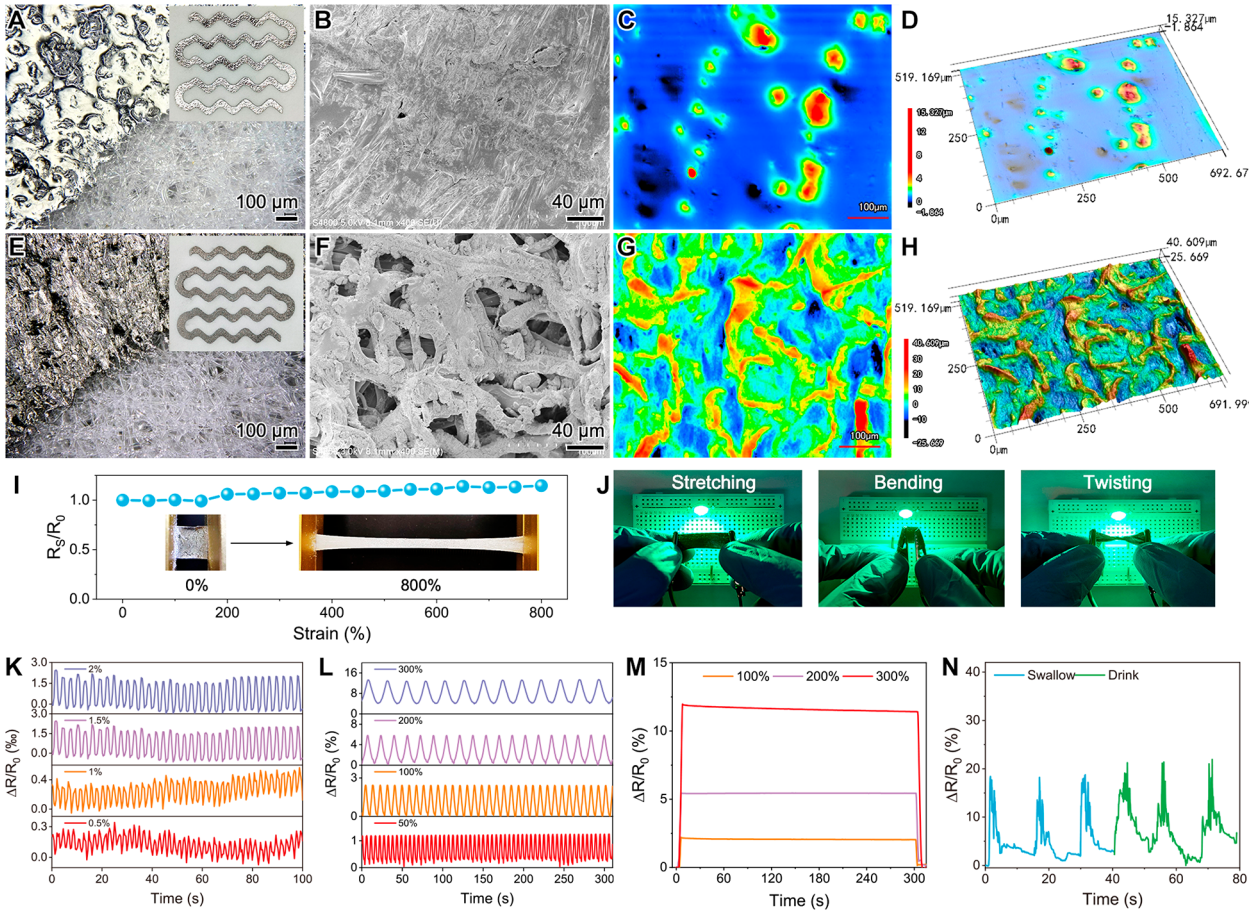

Figure 4. Optical microscopic images, SEM images, surface topographic images, and 3D contour maps of LM-printed SEBS fibers (A–D) before and (E–H) after mechanical activation. (I) The resistance change of the LM-casted Janus textile as a function of tensile strain. (J) Digital photographs of the Janus E-textile in an LED circuit under stretching, bending, and twisting deformations. The strain-sensing performance of the Janus E-textile (K,L) in different strain ranges of 0.5∼2% and 50∼300%. (M) Stability of static stretching under a strain range of 100∼300%. (N) Swallowing and drinking motion detection via a Janus E-textile.

on the SEBS/F127/LPs side and merely diffused around the hydrophilic surface (Figure 3E). More importantly, the SSFLP textile can maintain directional sweat transport capability under large strain (250%, Figure 3F) thanks to the ultraelastic and robust all-SEBS matrix. In practical, sweaty skin covered with a Janus SSFLP textile gets dry very quickly within minutes in an ambient environment (Figure 3G). The mechanism of fast perspiration-wicking is schematically described in Figure 3H; when the water droplet contacts the microfibers of SSFLP textile, it gets into the capillary channels, driven by the Laplace pressure (P_L):

$$P_L = \frac{4\gamma\cos\theta}{D} \tag{3}$$

where γ is the liquid–gas interfacial tension, θ is the water contact angle, and D is the pore diameter. The direction of the capillary force is determined by the negative or positive value of the Laplace pressure. Due to the asymmetric pore sizes and contact angles of SEBS and SEBS/F127/LPs layers, the P_L values of liquid droplets in two capillary channels vary. Immediately after the water gets into contact with the SEBS side, it will be absorbed into the pores of the textile by the Laplace pressure P_{L2}. In the interface between two layers, the sweat droplet is subjected to two Laplace pressures P_{L2} and P_{L1}, with the resultant force in the upward direction being $\Delta P = P_{L2} - P_{L1}$. Apparently, once the droplet comes into the hydrophobic SEBS fibers, the resultant force acting on it keeps constantly upward, leading to directional, nonreversible, and even antigravity liquid transportation. Reversely, when the water is dropped from above over the hydrophilic side of the Janus textile, the droplet will quickly spread out owing to the strong Laplace pressures (P_{L1}) and the downward hydrostatic pressure (HP). Yet, the liquid cannot penetrate the hydrophobic fibers of the SEBS layer due to the upward Laplace pressure difference, thus leading to sweat accumulation on the hydrophilic side.[33]

Applications in Personal Health Monitoring. Liquid metal with unrivaled electrical conductivity was stencil-printed on the bilayered nonwoven (onto the SEBS layer) to fabricate the Janus electronic textile. Figure 4A displays the microscopic and digital photographs of the freshly printed LM circuit with a silvery and shiny appearance lying on the SEBS microfibers. Evidently, the boundary between the LM and underlying SEBS fibers is clear and distinctive, so no excessive diffusion of LM can be observed. However, magnified SEM images reveal that the as-printed LM mainly covering the surface of the nonwoven in a bulk state, instead of penetrating the microporous matrix (Figure 4B). Further surface topographical measurements through laser microscopy also prove this morphology (Figure 4C,D). Such an inhomogeneous combi-

https://doi.org/10.1021/acs.nanolett.2c02647
Nano Lett. 2022, 22, 7597–7605

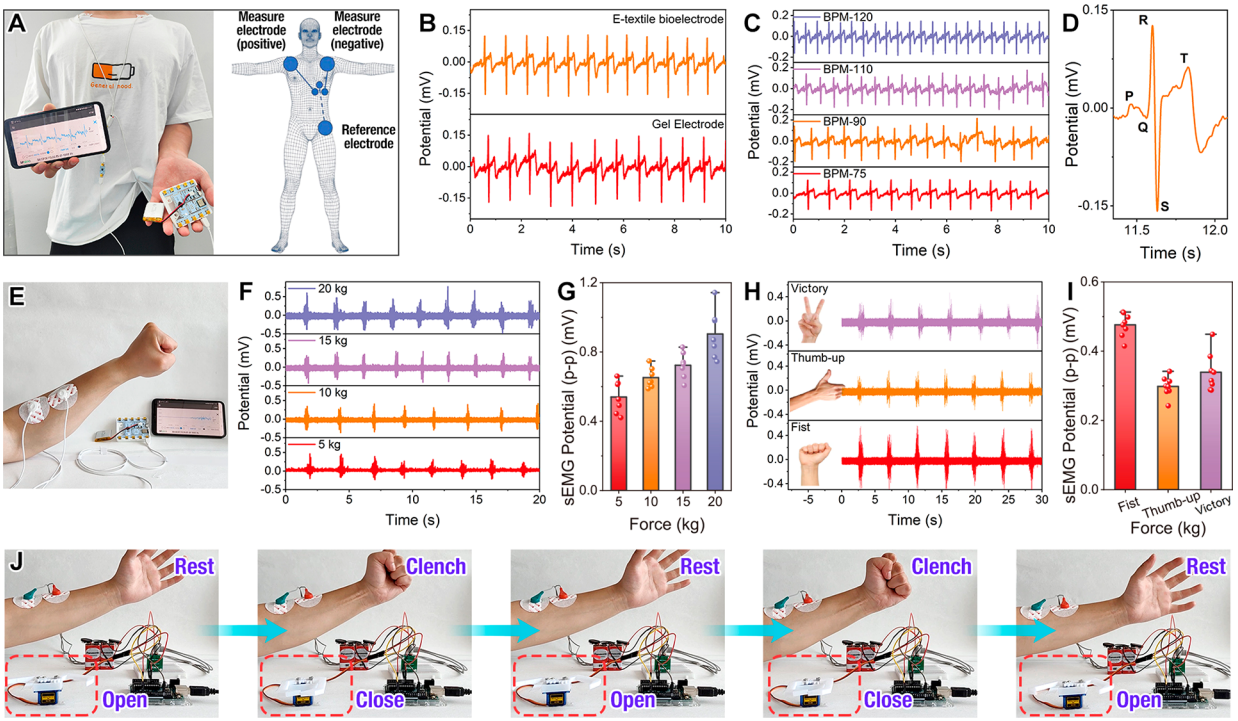

Figure 5. (A) Janus E-textile electrodes attached to a male volunteer for ECG acquisition. (B) ECG signals collected by the commercial gel electrodes and the E-textile bioelectrodes. (C) ECG signals recorded at a heartbeat rate from 75∼120 bpm. (D) Magnified ECG signals detected by the E-textile showing the distinct P, Q, R, S, and T waves. (E) Photograph of the sEMG monitoring setup. (F,G) sEMG potential and corresponding average peak values measured by the E-textile bioelectrodes at different gripping forces. (H,I) Gesture recognition by the E-textile and corresponding peak values. (J) HMI application of the E-textile electrodes in controlling a robotic claw using sEMG signals.

nation would inevitably cause circuit turnoff when applied for on-skin electronics. Herein, the as-printed LM circuit was activated via repeated monolithic stretching.[12] As a consequence, the shiny circuit converted to matte gray with no shifts of the boundary can be observed, showing good stability of the LM circuit (Figure 4E,F). Excitingly, the plain surface of the freshly printed LM was replaced by well-defined fibrous morphology, and the 3D contour map of the prestretched electronic textile implies that the fiber shapes as well as the porous structures were completely retained (Figure 4G,H), indicating the liquid metal was infiltrated into the fibrous matrix during mechanical stretching, thus guaranteeing its excellent and stable conductivity during large-scale deformation. Furthermore, the air and water moisture permeability of the bilayer textile experienced neglectable change after the LM circuit printing (Figure S5). As shown in Figure 4I, the electrical resistance increased by only 4.1% when the nonwoven was stretched to 800%. As a demonstration, one piece of Janus textile was applied as the wire was able to connect a circuit with an LED light under large tensile strain, bending, and twisting (Figure 4J).

The fabricated Janus electronic textile possesses superior stretchability and conductivity so that it can be directly used as on-skin strain sensors and bioelectrodes. We commenced measuring the strain-sensing behavior of the E-textile in cycles under varied tensile strains. It is found that the minimum detection of strains was as low as 0.5% (Figure 4K), while the resistance responses at large strains (50−300%) were stable and sound as well (Figure 4L). Moreover, the response and recovery times of the E-textile were determined to be 0.6 and 0.3 s (Figure S6), respectively, implying the fast installation of conducting paths in the liquid metal decorated microfibers. In addition, the drifting features of the sensor under static stretching of 100, 200, and 300% were investigated. As shown in Figure 4M, the resistance signals of the E-textile kept steady for over 300 s, demonstrating its outstanding conductive network as well as dependable sensing performance. The long-term working capability of the sensor was further proved by implementing 5000 continuous loading/unloading cycles at a fixed strain of 100% (Figure S7). Finally, the Janus E-textile was dressed on a volunteer to investigate its capability for human movement monitoring. As presented in Figure 4N, the sensor can readily capture the subtle motions of an Adam's apple so that the swallowing and drinking activities can be legibly detected. In short, the constructed perspiration-wicking Janus E-textile can be applied in the accurate and quick monitoring of human motions.

The low Young's modulus (36.5 kPa) of the conductive Janus E-textile leads to a comparable softness to that of human skin, combining with the remarkable electrical conductivity, making the E-textiles desirable bioelectrodes to record electrophysiology signals including ECG and sEMG. The ECG signals at different heartbeat rates from 70 to 120 bpm (at different exercising intensities) were recorded and shown in Figure 5A−D. Clearly, the biosignals collected by the E-textile bioelectrodes show equivalent high quality as the impermeable commercial gel electrodes. Electrical signals at varied heartbeats exhibit significant differences in terms of frequency and peak intensity, implying the accurate acquiring capability of the Janus E-textile for ECG signals. Apart from the ECG signals, another important physiological signal, namely, sEMG, was monitored using the Janus E-textile bioelectrode by mounting it onto the extensor digitorum (detection electrodes) and the elbow joint (reference electrode) (Figure 5E). The sEMG

https://doi.org/10.1021/acs.nanolett.2c02647
Nano Lett. 2022, 22, 7597−7605

signals of varied extensor contraction actions were monitored at different gripping forces. As displayed in Figure 5F,G, via repeatedly applying 5, 10, 15, and 20 kg of gripping force to the gripper, stable and reproducible electrical signals generated from the muscle activity can be detected under the same gripping force. More importantly, the E-textile bioelectrodes can monitor the steady increase in signal intensity. Low amplitude signal recognition and great output reliability make the Janus bioelectrodes capable of distinguishing different finger gestures via sEMG. As shown in Figure 5H,I, the E-textile could precisely identify the specific sEMG signal intensities and patterns for gestures "Strong" (fist clench), "Praise" (thumb-up), and "Victory" (index and middle fingers up). The signal reliability corresponding to each gesture was further confirmed by the repetition of three finger movements. Additionally, the signal-to-noise ratio (SNR) of the Janus E-textile was calculated according to the following equation:

$$\mathrm{SNR(dB)} = 20 \times \log_{10} \frac{\sqrt{\sum_{k=1}^{N} V_{\mathrm{signal}(k)}^2}}{\sqrt{\sum_{k=1}^{N} V_{\mathrm{noise}(k)}^2}} \quad (4)$$

Where N is the number of samples, $V_{\mathrm{signal}(k)}$ and $V_{\mathrm{noise}(k)}$ are the voltage values of the signal and noise, respectively. Hence, the SNR values for the ECG and sEMG signals were measured to be 18.0 and 23.2 dB, respectively. sEMG collected from different muscle contractions possesses wide applications in human−machine interfaces (HMIs). Herein, the sEMG signals generated by wrist flexors were utilized as a user interface to control a mechanical claw. The sEMG signals acquired by the E-textile electrodes were initially filtered and amplified using the signal processing unit and then supplied to the Arduino microcontroller unit to control the motor (Figure S8). Figure 5J and Video S4 show that the mechanical claw can be precisely and in real-time controlled under different forces of muscle contraction, indicating the potential of the Janus E-textiles in robotics and intelligent systems.

In summary, via an efficient electrospin-assisted face-to-face assembly and post LM stencil printing, an ultrastretchable and luminescent Janus electronic textile with directional sweat transport capability was successfully developed, which could be applied as an advanced epidermal electrode for long-term personal health management as well as HMIs. The asymmetric porosity and wettability synergistically boosted the perspiration-wicking and thus realized the long-term wearing comfort. Also, the phosphor $SrAl_2O_4$: Eu^{2+}, Dy^{3+} particles were well-embedded into the elastic fibers, empowering the electronic textile with excellent luminescent capability under extreme stretching in a dark environment. More importantly, the mechanically activated LM circuits exhibited excellent stability and conductivity under large strains (up to 900%), ensuring the high-quality recording of the biosignals and the precise control of a robotic claw. This research offers a promising alternative to producing advanced E-textiles for smart on-skin bioelectronics.

■ ASSOCIATED CONTENT

Supporting Information

The Supporting Information is available free of charge at https://pubs.acs.org/doi/10.1021/acs.nanolett.2c02647.

Additional experimental materials and methods, supplementary discussion on luminescence mechanism of $SrAl_2O_4$: Eu^{2+}, Dy^{3+}, discussion on the moisture and air permeability, detailed discussion on mechanical properties, extra discussion on FTIR and XRD characterizations, steel template for liquid metal printing, demonstration of water vapor permeability, FTIR spectra and XRD patterns, response and recovery times of the Janus E-textile when utilized as a strain sensor, long-term stability test on the E-textile strain sensor (PDF)

Video S1. Luminescence under stretching (MP4)

Video S2. Water transport from SEBS side (MP4)

Video S3. Water transport from SEBS/F127/LPs side (MP4)

Video S4. Human−machine interface application (MP4)

■ AUTHOR INFORMATION

Corresponding Authors

Yunpeng Huang − *Key Laboratory of Synthetic and Biological Colloids, Ministry of Education, School of Chemical and Material Engineering, Jiangnan University, Wuxi 214122, China;* orcid.org/0000-0002-8710-9062; Email: hypjnu@jiangnan.edu.cn

Tianxi Liu − *Key Laboratory of Synthetic and Biological Colloids, Ministry of Education, School of Chemical and Material Engineering, Jiangnan University, Wuxi 214122, China;* orcid.org/0000-0002-5592-7386; Email: txliu@jiangnan.edu.cn

Authors

Jiancheng Dong − *Key Laboratory of Synthetic and Biological Colloids, Ministry of Education, School of Chemical and Material Engineering, Jiangnan University, Wuxi 214122, China*

Yidong Peng − *Key Laboratory of Synthetic and Biological Colloids, Ministry of Education, School of Chemical and Material Engineering, Jiangnan University, Wuxi 214122, China*

Lei Pu − *Key Laboratory of Synthetic and Biological Colloids, Ministry of Education, School of Chemical and Material Engineering, Jiangnan University, Wuxi 214122, China*

Kangqi Chang − *Key Laboratory of Synthetic and Biological Colloids, Ministry of Education, School of Chemical and Material Engineering, Jiangnan University, Wuxi 214122, China*

Le Li − *Key Laboratory of Synthetic and Biological Colloids, Ministry of Education, School of Chemical and Material Engineering, Jiangnan University, Wuxi 214122, China*

Chao Zhang − *State Key Laboratory for Modification of Chemical Fibers and Polymer Materials, College of Materials Science and Engineering, Donghua University, Shanghai 201620, China;* orcid.org/0000-0003-1255-7183

Piming Ma − *Key Laboratory of Synthetic and Biological Colloids, Ministry of Education, School of Chemical and Material Engineering, Jiangnan University, Wuxi 214122, China;* orcid.org/0000-0002-4597-0639

Complete contact information is available at: https://pubs.acs.org/10.1021/acs.nanolett.2c02647

Author Contributions

The manuscript was written through contributions of all authors. All authors have given approval to the final version of the manuscript.

https://doi.org/10.1021/acs.nanolett.2c02647
Nano Lett. 2022, 22, 7597−7605

Notes

The authors declare no competing financial interest.

■ ACKNOWLEDGMENTS

This work is financially supported by the National Natural Science Foundation of China (21875033), the China Postdoctoral Science Foundation (2022M711355), the Natural Science Foundation of Jiangsu Province (BK20221540), the Shanghai Scientific and Technological Innovation Project (18JC1410600), the Program of the Shanghai Academic Research Leader (17XD1400100), the State Key Laboratory for Modification of Chemical Fibers and Polymer Materials, Donghua University, and the Postgraduate Research & Practice Innovation Program of Jiangsu Province (KYCX22_2317). We also appreciate greatly the instrumental characterization services provided by Central Laboratory, School of Chemical and Material Engineering, Jiangnan University.

■ REFERENCES

(1) Someya, T.; Amagai, M. Toward a new generation of smart skins. *Nat. Biotechnol.* **2019**, *37*, 382−388.
(2) Xu, L.; Huang, Z.; Deng, Z.; Du, Z.; Sun, T. L.; Guo, Z.-H.; Yue, K. A Transparent, Highly Stretchable, Solvent-Resistant, Recyclable Multifunctional Ionogel with Underwater Self-Healing and Adhesion for Reliable Strain Sensors. *Adv. Mater.* **2021**, *33*, 2105306.
(3) Pu, L.; Liu, Y.; Li, L.; Zhang, C.; Ma, P.; Dong, W.; Huang, Y.; Liu, T. Polyimide Nanofiber-Reinforced Ti3C2Tx Aerogel with "Lamella-Pillar" Microporosity for High-Performance Piezoresistive Strain Sensing and Electromagnetic Wave Absorption. *ACS Appl. Mater. Interfaces* **2021**, *13*, 47134−47146.
(4) Dong, J.; Li, L.; Zhang, C.; Ma, P.; Dong, W.; Huang, Y.; Liu, T. Ultra-highly stretchable and anisotropic SEBS/F127 fiber films equipped with an adaptive deformable carbon nanotube layer for dual-mode strain sensing. *J. Mater. Chem. A* **2021**, *9*, 18294−18305.
(5) Dong, J.; Wang, D.; Peng, Y.; Zhang, C.; Lai, F.; He, G.; Ma, P.; Dong, W.; Huang, Y.; Parkin, I. P.; Liu, T. Ultra-stretchable and superhydrophobic textile-based bioelectrodes for robust self-cleaning and personal health monitoring. *Nano Energy* **2022**, *97*, 107160.
(6) Someya, T.; Bao, Z.; Malliaras, G. G. The rise of plastic bioelectronics. *Nature* **2016**, *540*, 379−385.
(7) Qiao, Y.; Li, X.; Wang, J.; Ji, S.; Hirtz, T.; Tian, H.; Jian, J.; Cui, T.; Dong, Y.; Xu, X.; Wang, F.; Wang, H.; Zhou, J.; Yang, Y.; Someya, T.; Ren, T.-L. Intelligent and Multifunctional Graphene Nanomesh Electronic Skin with High Comfort. *Small* **2022**, *18*, 2104810.
(8) Pu, L.; Ma, H.; Dong, J.; Zhang, C.; Lai, F.; He, G.; Ma, P.; Dong, W.; Huang, Y.; Liu, T. Xylem-Inspired Polyimide/MXene Aerogels with Radial Lamellar Architectures for Highly Sensitive Strain Detection and Efficient Solar Steam Generation. *Nano Lett.* **2022**, *22*, 4560−4568.
(9) He, X.; Shi, J.; Hao, Y.; Wang, L.; Qin, X.; Yu, J. PEDOT:PSS/CNT composites based ultra-stretchable thermoelectrics and their application as strain sensors. *Compos. Commun.* **2021**, *27*, 100822.
(10) Chang, K.; Li, L.; Zhang, C.; Ma, P.; Dong, W.; Huang, Y.; Liu, T. Compressible and robust PANI sponge anchored with erected MXene flakes for human motion detection. *Composites, Part A* **2021**, *151*, 106671.
(11) Chen, F.; Huang, Q.; Zheng, Z. Permeable conductors for wearable and on-skin electronics. *Small Struct.* **2022**, *3*, 2100135.
(12) Ma, Z.; Huang, Q.; Xu, Q.; Zhuang, Q.; Zhao, X.; Yang, Y.; Qiu, H.; Yang, Z.; Wang, C.; Chai, Y.; Zheng, Z. Permeable superelastic liquid-metal fibre mat enables biocompatible and monolithic stretchable electronics. *Nat. Mater.* **2021**, *20*, 859−868.
(13) He, J.; Lu, C.; Jiang, H.; Han, F.; Shi, X.; Wu, J.; Wang, L.; Chen, T.; Wang, J.; Zhang, Y.; Yang, H.; Zhang, G.; Sun, X.; Wang, B.; Chen, P.; Wang, Y.; Xia, Y.; Peng, H. Scalable production of high-performing woven lithium-ion fibre batteries. *Nature* **2021**, *597*, 57−63.
(14) Jia, C.; Xia, Y.; Zhu, Y.; Wu, M.; Zhu, S.; Wang, X. High-Brightness, High-Resolution, and Flexible Triboelectrification-Induced Electroluminescence Skin for Real-Time Imaging and Human−Machine Information Interaction. *Adv. Funct. Mater.* **2022**, *32*, 2201292.
(15) Barbosa, R.; Gupta, S. K.; Srivastava, B. B.; Villarreal, A.; De Leon, H.; Peredo, M.; Bose, S.; Lozano, K. Bright and persistent green and red light-emitting fine fibers: A potential candidate for smart textiles. *J. Lumin.* **2021**, *231*, 117760.
(16) Guo, Z.; Huang, G.; Zhang, C.; Luo, D.; Ye, T.; Chen, X. Facile engineering of cesium copper halide composites films with highly ambient stability and tunable optics performance. *Compos. Commun.* **2021**, *28*, 100949.
(17) Shi, X.; Zuo, Y.; Zhai, P.; Shen, J.; Yang, Y.; Gao, Z.; Liao, M.; Wu, J.; Wang, J.; Xu, X.; Tong, Q.; Zhang, B.; Wang, B.; Sun, X.; Zhang, L.; Pei, Q.; Jin, D.; Chen, P.; Peng, H. Large-area display textiles integrated with functional systems. *Nature* **2021**, *591*, 240−245.
(18) Son, D.; Kang, J.; Vardoulis, O.; Kim, Y.; Matsuhisa, N.; Oh, J. Y.; To, J. W. F.; Mun, J.; Katsumata, T.; Liu, Y.; McGuire, A. F.; Krason, M.; Molina-Lopez, F.; Ham, J.; Kraft, U.; Lee, Y.; Yun, Y.; Tok, J. B. H.; Bao, Z. An integrated self-healable electronic skin system fabricated via dynamic reconstruction of a nanostructured conducting network. *Nat. Nanotechnol.* **2018**, *13*, 1057−1065.
(19) Zhuang, Y.; Xie, R.-J. Mechanoluminescence Rebrightening the Prospects of Stress Sensing: A Review. *Adv. Mater.* **2021**, *33*, 2005925.
(20) Lee, J. I.; Choi, H.; Kong, S. H.; Park, S.; Park, D.; Kim, J. S.; Kwon, S. H.; Kim, J.; Choi, S. H.; Lee, S. G.; Kim, D. H.; Kang, M. S. Visco-Poroelastic Electrochemiluminescence Skin with Piezo-Ionic Effect. *Adv. Mater.* **2021**, *33*, 2100321.
(21) Huang, K.; Le, N.; Wang, J. S.; Huang, L.; Zeng, L.; Xu, W.-C.; Li, Z.; Li, Y.; Han, G. Designing Next Generation of Persistent Luminescence: Recent Advances in Uniform Persistent Luminescence Nanoparticles. *Adv. Mater.* **2022**, *34*, 2107962.
(22) Abdollahi, A.; Roghani-Mamaqani, H.; Razavi, B.; Salami-Kalajahi, M. Photoluminescent and Chromic Nanomaterials for Anticounterfeiting Technologies: Recent Advances and Future Challenges. *ACS Nano* **2020**, *14*, 14417−14492.
(23) Kabe, R.; Adachi, C. Organic long persistent luminescence. *Nature* **2017**, *550*, 384−387.
(24) Poelman, D.; Smet, P. F. Photometry in the dark: time dependent visibility of low intensity light sources. *Opt. Express* **2010**, *18*, 26293−26299.
(25) Botterman, J.; Smet, P. F. Persistent phosphor SrAl2O4:Eu,Dy in outdoor conditions: saved by the trap distribution. *Opt. Express* **2015**, *23*, A868−A881.
(26) Pang, C.; Koo, J. H.; Nguyen, A.; Caves, J. M.; Kim, M.-G.; Chortos, A.; Kim, K.; Wang, P. J.; Tok, J. B. H.; Bao, Z. Highly Skin-Conformal Microhairy Sensor for Pulse Signal Amplification. *Adv. Mater.* **2015**, *27*, 634−640.
(27) Jiang, N.; Li, H.; Hu, D.; Xu, Y.; Hu, Y.; Zhu, Y.; Han, X.; Zhao, G.; Chen, J.; Chang, X.; Xi, M.; Yuan, Q. Stretchable strain and temperature sensor based on fibrous polyurethane film saturated with ionic liquid. *Compos. Commun.* **2021**, *27*, 100845.
(28) Fan, C.; Wang, D.; Huang, J.; Ke, H.; Wei, Q. A highly sensitive epidermal sensor based on triple-bonded hydrogels for strain/pressure sensing. *Compos. Commun.* **2021**, *28*, 100951.
(29) Wang, Y.; Lee, S.; Yokota, T.; Wang, H.; Jiang, Z.; Wang, J.; Koizumi, M.; Someya, T. A durable nanomesh on-skin strain gauge for natural skin motion monitoring with minimum mechanical constraints. *Sci. Adv.* **2020**, *6*, No. eabb7043.
(30) Wang, H. L.; Guo, Z. H.; Pu, X.; Wang, Z. L. Ultralight Iontronic Triboelectric Mechanoreceptor with High Specific Outputs for Epidermal Electronics. *Nano-Micro Lett.* **2022**, *14*, 86.
(31) Zheng, S.; Li, W.; Ren, Y.; Liu, Z.; Zou, X.; Hu, Y.; Guo, J.; Sun, Z.; Yan, F. Moisture-wicking, Breathable and Intrinsically Anti-

https://doi.org/10.1021/acs.nanolett.2c02647
Nano Lett. 2022, 22, 7597−7605

bacterial Electronic Skin Based on Dual Gradient poly(ionic liquid) Nanofiber Membranes. *Adv. Mater.* **2022**, *34*, 2106570.
(32) Yamamoto, H.; Matsuzawa, T. Mechanism of long phosphorescence of SrAl2O4:Eu2+, Dy3+ and CaAl2O4:Eu2+, Nd3+. *J. Lumin.* **1997**, *72*−*74*, 287−289.
(33) He, X.; Yang, S.; Pei, Q.; Song, Y.; Liu, C.; Xu, T.; Zhang, X. Integrated Smart Janus Textile Bands for Self-Pumping Sweat Sampling and Analysis. *ACS Sens.* **2020**, *5*, 1548−1554.

https://doi.org/10.1021/acs.nanolett.2c02647
Nano Lett. 2022, 22, 7597−7605